Katholieke Universiteit Leuven

Departement Elektrotechniek ESAT-SISTA/TR 2006-153

Feedback control in hearing aids [1]

Ann Spriet[2], Simon Doclo[3] ,Marc Moonen[4] ,Jan Wouters[5]

Springer Handbook of Speech Processing and Speech Communication (Chapter 48, Part H. Speech Enhancement) (Benesty J., Huang, Y. A., Sondhi, M., eds.), Springer, 2007.

[1]This report is available by anonymous ftp from *ftp.esat.kuleuven.ac.be* in the directory *pub/sista/spriet/reports/06-153.pdf*

[2]K.U.Leuven, Dept. of Electrical Engineering (ESAT), SISTA, Kasteelpark Arenberg 10, 3001 Leuven-Heverlee, Belgium, Tel. 32/16/32 17 95, Fax 32/16/32 19 70. K.U.Leuven, ExpORL, Dept. Neurosciences, O.& N2, Herestraat 49 bus 721, B-3000 Leuven, Belgium. Ann Spriet is a postdoctoral researcher supported by FWO-Vlaanderen.

[3]K.U.Leuven, Dept. of Electrical Engineering (ESAT), SISTA, Kasteelpark Arenberg 10, 3001 Leuven-Heverlee, Belgium, Tel. 32/16/32 18 99, Fax 32/16/32 19 70.

[4]K.U.Leuven, Dept. of Electrical Engineering (ESAT), SISTA, Kasteelpark Arenberg 10, 3001 Heverlee, Belgium, Tel. 32/16/32 17 09, Fax 32/16/32 19 70. Marc Moonen is a professor at the Katholieke Universiteit Leuven.

[5]K.U.Leuven, ExpORL, Dept. Neurosciences, O.& N2, Herestraat 49 bus 721, B-3000 Leuven, Belgium, Tel: +32 16 330485, Fax: +32 16 330486 Jan Wouters is a professor at the Katholieke Universiteit Leuven.

FEEDBACK CONTROL IN HEARING AIDS

Ann Spriet[†,‡]*, Simon Doclo*[†]*, Marc Moonen*[†] *and Jan Wouters*[‡]

[†] K.U.Leuven, ESAT-SCD
Kasteelpark Arenberg 10
B-3001 Leuven, Belgium
{spriet,doclo,moonen}@esat.kuleuven.be

[‡] K.U.Leuven, ExpORL
Dept. Neurosciences
O.&N2, Herestraat 49, bus 721
B-3000 Leuven, Belgium
jan.wouters@med.kuleuven.be

Acoustic feedback limits the maximum amplification that can be used in a hearing aid without making it unstable. This chapter gives an overview of existing techniques for feedback suppression and, in particular, adaptive feedback cancellation. Because of the presence of a closed signal loop, standard adaptive filtering techniques for open-loop systems fail to provide a reliable feedback path estimate if the desired signal is spectrally colored. Several approaches for improving the estimation accuracy of the adaptive feedback canceller will be reviewed and evaluated for acoustic feedback paths measured in a commercial behind-the-ear hearing aid.

1. INTRODUCTION

Acoustic feedback in hearing aids refers to the acoustical coupling between the loudspeaker and the microphone of the hearing aid. Because of this coupling, the hearing aid produces a severe distortion of the desired signal and an annoying howling sound when the gain is increased. With the growing use of open fittings, i.e., without an earmold, and the decreasing distance between the loudspeaker and the microphone of the hearing aid, the demand for effective feedback suppression or cancellation techniques increases.

This chapter gives an overview of existing techniques for feedback suppression and, in particular, adaptive feedback cancellation. Because of the presence of a closed signal loop, the standard adaptive filtering techniques for open-loop systems (as used in echo cancellation) fail to provide a reliable feedback path estimate if the desired signal is spectrally colored. Several approaches for improving the estimation accuracy of the adaptive feedback canceller will be discussed.

This chapter is organized as follows. Section 2 gives a mathematical formulation of the acoustic feedback problem in hearing aids and briefly describes the two possible approaches to reduce its negative effects, i.e., feedforward suppression and feedback cancellation. In addition, performance measures for feedback cancellation are defined.

Section 3 discusses the standard continuous adaptation feedback cancellation (CAF) algorithm that is widely studied for application in hearing aids. We demonstrate that the standard CAF suffers from a model error or bias when the desired signal is spectrally colored (e.g., a speech signal).

In the literature, several solutions have been proposed to reduce the bias of the CAF. A common approach is to incorporate signal decorrelating operations (such as delays) in the signal processing path of the hearing aid or to reduce the adaptation speed of the adaptive feedback canceller. Other techniques, discussed in Section 4, exploit prior knowledge of the acoustic feedback path to improve the adaptation of the feedback canceller. In Section 5, a final class of techniques is presented that view the feedback path as a part of a closed-loop system and apply closed-loop system identification theory [1]. Among the different closed-loop identification methods, especially the direct method is an appealing approach for feedback cancellation. In contrast to the other methods, this technique does not require the use of an external

probe signal. The direct method reduces the bias of the feedback canceller by incorporating a (stationary or time-varying) model of the desired signal $x[k]$ in the identification.

Finally, Section 6 compares the steady-state performance as well as the tracking performance of different algorithms for acoustic feedback paths measured in a commercial behind-the-ear hearing aid.

2. PROBLEM STATEMENT

Section 2.1 defines the notation and gives a mathematical formulation of the acoustic feedback problem in hearing aids. Section 2.2 describes the two approaches that can be used to reduce acoustic feedback, i.e., feedforward suppression and feedback cancellation. In Section 2.3, we define the performance measures that will be used to evaluate the feedback cancellation techniques.

2.1. Acoustic feedback in hearing aids

Notation

The superscripts T and H denote matrix/vector transpose and complex conjugate transpose, respectively. The expectation operator is denoted by $\mathcal{E}\{\cdot\}$. The matrix $\mathcal{F}$ is the $M \times M$ Discrete Fourier Transform (DFT) matrix. The matrix $\mathbf{I}_L$ is the $L \times L$ identity matrix; The matrix $\mathbf{0}_L$ is an $L \times L$ dimensional matrix of zeros.

The discrete-time index is denoted by k. The symbol q^{-1} denotes the discrete-time delay operator, i.e.,

$$q^{-1}u[k] = u[k-1]. \tag{1}$$

A discrete-time filter with coefficient vector $\mathbf{f}[k]$

$$\mathbf{f}[k] = \left[\ f_0[k]\ \ f_1[k]\ \ \cdots\ \ f_{L_F-1}[k]\ \right]^T \tag{2}$$

and filter length L_F is represented as a polynomial transfer function $F(q,k)$ in q, i.e.,

$$F(q,k)=\mathbf{f}^T[k]\mathbf{q}, \tag{3}$$

with $\mathbf{q} = \left[\ 1\ \ q^{-1}\ \ \ldots\ \ q^{-L_F+1}\ \right]^T$. This representation, which is adopted from [2], allows the following notation for the filtering of $u[k]$ with $F(q,k)$:

$$F(q,k)u[k]\ =\ \mathbf{f}^T[k]\mathbf{u}[k], \tag{4}$$

with

$$\mathbf{u}[k]=\left[u[k]\ \ u[k-1]\ \ \cdots\ \ u[k-L_F+1]\right]^T. \tag{5}$$

The spectrum of $F(q,k)$ is denoted by $F(e^{j\omega},k)$ with $\omega \in [0,\pi]$ the normalized angular frequency.

Acoustic feedback

Figure 1 illustrates the problem of acoustic feedback for a hearing aid with a single microphone. The so-called *forward path* $G(q,k)$ represents the regular signal processing path of the hearing aid, typically including a frequency specific gain, compression and/or noise reduction. We assume that $G(q,k)$ has a delay d_G of at least one sample, i.e., $g_0 = 0$.

The *feedback path* between the loudspeaker and the microphone is denoted by $F(q,k)$. It includes the frequency characteristic of the loudspeaker and the microphone, the acoustic feedback path and the characteristics of the digital-to-analog (DAC) and analog-to-digital (ADC) converters. The feedback path $F(q,k)$ typically contains a delay d_F that arises from the processing delay of the ADC and DAC converters and the propagation time of the sound from the loudspeaker to the microphone. For simplicity, we will include this delay d_F in the delay d_G of the forward path $G(q,k)$. The loudspeaker and microphone signal are $u[k]$ and $y[k]$, respectively. The desired sound signal (i.e., without acoustic feedback) is denoted by $x[k]$ and the feedback signal is denoted by $n[k] = F(q,k)u[k]$.

Ideally, the loudspeaker signal $u[k]$ equals the desired signal $x[k]$ processed by the forward path $G(q,k)$, i.e.,

$$u[k] = G(q,k)x[k]. \tag{6}$$

However, because of acoustic feedback, the amplified sound $u[k]$ sent through the loudspeaker is fed back into the microphone, resulting in a closed-loop system $C(q,k)$

$$C(q,k) = \frac{G(q,k)}{1 - G(q,k)F(q,k)} \tag{7}$$

from $x[k]$ to the loudspeaker signal $u[k]$.

Instability occurs if the loop gain $\left|G(e^{j\omega},k)F(e^{j\omega},k)\right|$ exceeds one at an angular

frequency $\omega \in [0, \pi]$ with positive feedback, i.e., an angular frequency where the loop phase $\angle \big(G(e^{j\omega}, k)F(e^{j\omega}, k)\big)$ equals a multiple of 2π. If the gain $|G(e^{j\omega}, k)|$ is increased beyond this point, the system starts to oscillate. However also at low gain margins, acoustic feedback already degrades the sound quality by introducing ringing or howling. To avoid significant audible distortion, a gain margin of at least 6 dB is advisable: the effect of the acoustic feedback on the closed-loop frequency response $C(e^{j\omega}, k)$ is then limited to [3]

$$\frac{2}{3}G(e^{j\omega}, k) \leq C(e^{j\omega}, k) \leq 2G(e^{j\omega}, k). \quad (8)$$

As an illustration, Figure 2 depicts the feedback path frequency response measured in a commercial, GN ReSound behind-the-ear hearing aid. During the measurement, the hearing aid was attached to the right ear of a Cortex MK II artificial head. An earmold with a vent size of 2 mm was used. In this example, the minimum feedback path attenuation, and hence, the maximum amplification without instability lies around 20 dB. The acoustic feedback path when a mobile phone is attached to the head is also shown. This demonstrates that placing a telephone handset close to the ear can temporarily reduce the feedback path attenuation by another 10 to 20 dB [4, 5, 6].

2.2. Feedforward suppression versus feedback cancellation

To reduce the negative effects introduced by acoustic feedback, several techniques have been proposed in the literature. They can be broadly classified into feedforward suppression and feedback cancellation techniques.

Feedforward suppression

In *feedforward suppression* techniques, the regular signal processing path $G(q, k)$ of the hearing aid is modified in such a way that it is stable in conjunction with the feedback path $F(q, k)$. The most common technique is the use of a notch filter . In a notch filter, the gain is reduced in a narrow frequency band around the critical frequencies, whenever feedback occurs [7, 8, 9, 10]. The main disadvantage is that this approach is reactive: in order to identify the oscillation frequencies, howling first has to occur. Other examples include equalizing the phase of the open-loop response [11] and using time-varying elements (such as frequency shifting, delay and phase modulation) in the forward path $G(q, k)$ [7, 12, 13].

The achievable increase in maximum stable gain with feedforward suppression techniques was generally found to be limited [7, 12]. In addition, feedforward suppression techniques all compromise the basic frequency response of the hearing aid, and hence, may seriously affect the sound quality.

Feedback cancellation

A more promising solution for acoustic feedback is the use of a *feedback cancellation* algorithm, which is described in Figure 3. The feedback canceller $\hat{F}(q, k)$ produces an estimate $z[k]$ of the feedback signal $n[k]$ and subtracts this estimate $z[k]$ from the microphone signal $y[k]$. As a result, the closed-loop transfer function $C(q, k)$ from the desired signal $x[k]$ to the loudspeaker signal $u[k]$ is modified into

$$C(q, k) = \frac{G(q, k)}{1 - G(q, k)\left(F(q, k) - \hat{F}(q, k)\right)}. \quad (9)$$

Ideally, $\hat{F}(q, k) = F(q, k)$ such that the closed-loop system $C(q, k)$ equals the desired hearing aid response $G(q, k)$.

The acoustic path $F(q, k)$ between the loudspeaker and the microphone can vary significantly depending on the acoustical environment (see Figure 2) [4, 5, 6, 14]. Hence, adaptive feedback cancellers $\hat{F}(q, k)$ are called for. In the remainder of this chapter, existing adaptive feedback cancellation techniques will be discussed.

2.3. Performance of a feedback canceller

The most common measures to assess the performance of feedback cancellation algorithms are the misalignment between the true and estimated feedback path $\hat{F}(q, k)$ and the maximum stable gain [14, 15, 16, 17, 18].

The *misalignment* $\zeta_k(F, \hat{F})$ between the true feedback path $F(q, k)$ and the feedback path estimate $\hat{F}(q, k)$ is computed in the frequency-domain as

$$\zeta_k(F,\hat{F}) = \sqrt{\frac{\int_0^{\pi} \left| F(e^{j\omega},k) - \hat{F}(e^{j\omega},k) \right|^2 d\omega}{\int_0^{\pi} |F(e^{j\omega},k)|^2 d\omega}}. \quad (10)$$

The misalignment reflects the accuracy of the feedback path estimate $\hat{F}(q,k)$.

To get an idea of the actual benefit of a feedback cancellation algorithm for the hearing aid user, the *maximum stable gain* (MSG) is often used [16, 14]. In this chapter, the MSG is defined as the largest gain for which the hearing aid does not oscillate and the desired signal is not substantially degraded by algorithm artefacts (e.g., signal distortion or howling) [16]. The MSG is determined by gradually and slowly increasing the gain while the feedback canceller is running.

3. STANDARD ADAPTIVE FEEDBACK CANCELLER

Adaptive feedback cancellers can be divided into two classes: algorithms with a continuous adaptation and algorithms with a *non-continuous adaptation* [9, 16, 19]. The latter only adapt the coefficients of the feedback canceller when instability is detected or when the input signal level is low [19, 20, 21]. Due to this reactive, rather than proactive, adaptation, such systems may be objectionable. A *continuous adaptation* feedback canceller, on the other hand, continuously adapts the coefficients of the feedback canceller.

This section describes a standard continuous adaptation feedback cancellation (CAF) technique that is widely studied for hearing aid applications [9, 16, 22]. In Section 3.2, we show that because of the presence of a closed signal loop, the standard CAF suffers from a large model error or bias, if the desired signal is spectrally colored. Classical approaches for reducing the bias of the CAF are discussed in Section 3.3.

3.1. Adaptation of the CAF

The CAF continuously adapts the coefficients

$$\hat{\mathbf{f}}[k] = [\ f_0[k]\ \ f_1[k]\ \ \cdots\ \ f_{L_{\hat{F}}-1}[k]\ ]^T \quad (11)$$

of the feedback canceller based on standard adaptive filtering (Wiener filtering) procedures (see Figure 3). The CAF minimizes the energy of the feedback compensated signal e[k], i.e.,

$$J(\hat{\mathbf{f}}[k]) = \mathcal{E}\left\{ \left| y[k] - \hat{\mathbf{f}}^T[k]\mathbf{u}[k] \right|^2 \right\}, \quad (12)$$

with

$$\mathbf{u}[k] = [\ u[k]\ \ \cdots\ \ u[k - L_{\hat{F}} + 1]\ ]^T, \quad (13)$$

resulting in the well-known Wiener filter

$$\hat{\mathbf{f}}[k] \ = \ \mathcal{E}\{\mathbf{u}[k]\mathbf{u}^T[k]\}^{-1}\mathcal{E}\{\mathbf{u}[k]y[k]\}. \quad (14)$$

Assuming the sufficient-order case where $L_{\hat{F}} = L_F$ and using

$$y[k] = \mathbf{f}^T[k]\mathbf{u}[k] + x[k], \quad (15)$$

(14) can be written as:

$$\begin{aligned} \hat{\mathbf{f}}[k] \ &= \ \mathcal{E}\{\mathbf{u}[k]\mathbf{u}^T[k]\}^{-1}\mathcal{E}\{\mathbf{u}[k]\mathbf{u}^T[k]\mathbf{f}[k]\} \\ &\quad +\mathcal{E}\{\mathbf{u}[k]\mathbf{u}^T[k]\}^{-1}\mathcal{E}\{\mathbf{u}[k]x[k]\}. \\ &= \ \mathbf{f}[k]+\mathcal{E}\{\mathbf{u}[k]\mathbf{u}^T[k]\}^{-1}\mathcal{E}\{\mathbf{u}[k]x[k]\}. \end{aligned} \quad (16)$$

From (16), it can be seen that the desired signal $x[k]$ acts as a disturbance to the feedback canceller.

Standard adaptive filter procedures (e.g., Least Mean Squares (LMS), Recursive Least Squares (RLS)) can be used for adapting the filter coefficients $\hat{\mathbf{f}}[k]$.

Time-domain Normalized LMS (NLMS)

The most popular adaptive filtering technique is the NLMS algorithm, i.e.,

$$\begin{aligned} \hat{\mathbf{f}}[k] \ &= \ \hat{\mathbf{f}}[k-1] + \\ &\quad \mu[k]\mathbf{u}[k]\Big(y[k] - \hat{\mathbf{f}}^T[k-1]\mathbf{u}[k]\Big). \end{aligned} \quad (17)$$

Unlike in acoustic echo cancellation, the feedback canceller adapts during a continuous double-talk situation (see (16)). To reduce the excess mean square error (MSE) in the presence of desired signals $x[k]$ with large power fluctuations or signal onsets, the step size $\mu[k]$ of the NLMS algorithm is normalized

with to the sum of the short-term average input power $\overline{|u[k]|^2}$ and error power $\overline{|e[k]|^2}$ [16, 23]:

$$\mu[k] = \frac{\bar{\mu}}{L_{\hat{F}}\left(\overline{|u[k]|^2} + \overline{|e[k]|^2}\right) + c}, \quad (18)$$

where $\bar{\mu}$ is a dimensionless step size constant, c is a small positive constant to prevent singularities and

$$\overline{|u[k]|^2} = (1-\gamma)|u[k]|^2 + \gamma\overline{|u[k-1]|^2}, \quad (19)$$
$$\overline{|e[k]|^2} = (1-\gamma)|e[k]|^2 + \gamma\overline{|e[k-1]|^2}, \quad (20)$$

with $\gamma \in (0,1]$. For a highly time-varying signal $x[k]$ such as a speech signal, a burst in $e[k]$ most often originates from an increase in the short-term power of $x[k]$. Hence, normalization with the error power reduces the step size $\mu[k]$ when the desired signal $x[k]$ is strong and thus mitigates the negative effect of a strong desired signal segment on the excess MSE.

Partitioned-block frequency-domain NLMS

Better performance can be achieved when updating the feedback canceller in the frequency-domain [24, 25, 26, 27]. Partitioned-block frequency-domain (PBFD) adaptive filters combine the beneficial properties of frequency-domain algorithms, i.e., a faster convergence (thanks to a frequency-dependent step size control) and a reduced complexity, with a small processing delay as required for hearing aids.

In this chapter, we concentrate on a PBFD implementation based on overlap-save [27]. In this implementation, the $L_{\hat{F}}$-taps feedback canceller $\hat{\mathbf{f}}[k]$ is partitioned in $\frac{L_{\hat{F}}}{P}$ segments $\hat{\mathbf{f}}_p[k]$ of length P each. Each segment $\hat{\mathbf{f}}_p[k]$, $p = 0, \ldots, \frac{L_{\hat{F}}}{P} - 1$ is then transformed to the frequency-domain vector $\hat{\mathbf{F}}_p[k]$ by means of the M-point DFT matrix $\boldsymbol{\mathcal{F}}$:[1]

$$\hat{\mathbf{f}}_p[k] = \left[\ \hat{f}_{pP}[k] \ \ldots \ \hat{f}_{(p+1)P-1}[k]\ \right]^T, \quad (21)$$
$$\hat{\mathbf{F}}_p[k] = \boldsymbol{\mathcal{F}}\begin{bmatrix}\hat{\mathbf{f}}_p[k]\\ \mathbf{0}\end{bmatrix}\begin{matrix}\updownarrow P\\ \updownarrow M-P\end{matrix}. \quad (22)$$

Let the L dimensional block signal $\mathbf{u}_{\bar{k}}$ be defined as

$$\mathbf{u}_{\bar{k}} = \left[\ u[\bar{k}L+1] \ \ldots \ u[(\bar{k}+1)L]\ \right]^T, \quad (23)$$

[1] It is assumed that $\frac{L_{\hat{F}}}{P} \in \mathbb{N}_0$. Otherwise $\hat{\mathbf{f}}_p[k]$ has to be padded with zeros.

with $\bar{k}$ the block index. For each block of L input samples $\mathbf{u}_{\bar{k}}$, the PBFD NLMS filter produces L output samples $\mathbf{z}_{\bar{k}} = \left[z[\bar{k}L+1] \ \ldots \ z[(\bar{k}+1)L]\right]^T$:

$$\mathbf{U}_p[\bar{k}] = \mathrm{diag}\left\{\boldsymbol{\mathcal{F}}\begin{bmatrix}u[(\bar{k}+1)L - pP - M + 1]\\ \vdots \\ u[(\bar{k}+1)L - pP]\end{bmatrix}\right\}, \quad (24)$$

$$\mathbf{z}_{\bar{k}} = \left[\ \mathbf{0}\ \ \mathbf{I}_L\ \right]\boldsymbol{\mathcal{F}}^{-1}\sum_{p=0}^{\frac{L_{\hat{F}}}{P}-1}\mathbf{U}_p[\bar{k}]\hat{\mathbf{F}}_p[\bar{k}]. \quad (25)$$

The parameter L is called the block length and hence, the corresponding input/output delay of the PBFD implementation equals $2L-1$. To ensure proper operation, it is required that the DFT-length $M \geq P + L - 1$.

The PBFD update equation equals:

$$\hat{\mathbf{F}}_p[\bar{k}+1] = \hat{\mathbf{F}}_p[\bar{k}] + \boldsymbol{\Delta}[\bar{k}]\boldsymbol{\mathcal{F}}\mathbf{g}\boldsymbol{\mathcal{F}}^{-1}\mathbf{U}_p^H[\bar{k}]\mathbf{E}[\bar{k}], \quad (26)$$

where

$$\mathbf{E}[\bar{k}] = \boldsymbol{\mathcal{F}}\begin{bmatrix}\mathbf{0}\\ \mathbf{I}_L\end{bmatrix}(\mathbf{y}_{\bar{k}} - \mathbf{z}_{\bar{k}}), \quad (27)$$
$$\mathbf{y}_{\bar{k}} = \left[\ y[\bar{k}L+1] \ \ldots \ y[(\bar{k}+1)L]\ \right]^T, \quad (28)$$

and

$$\mathbf{g} = \begin{bmatrix}\mathbf{I}_P & \mathbf{0}\\ \mathbf{0} & \mathbf{0}_{M-P}\end{bmatrix}. \quad (29)$$

The matrix $\boldsymbol{\Delta}[\bar{k}]$ in (26) is a diagonal matrix that contains the step sizes $\mu_m[\bar{k}]$, $m = 0, \ldots, M-1$ of the different frequency bins m, i.e.,

$$\boldsymbol{\Delta}[\bar{k}] = \mathrm{diag}\{\mu_0[\bar{k}], \ldots, \mu_{M-1}[\bar{k}]\}. \quad (30)$$

Each step size $\mu_m[\bar{k}]$ is normalized according to the sum of the input and the error power in each frequency bin m:

$$\mu_m[\bar{k}] = \frac{\bar{\mu}_m}{\sum_{p=0}^{\frac{L_{\hat{F}}}{P}-1}\left|U_{p,m}[\bar{k}]\right|^2 + \frac{L_{\hat{F}}}{P}\left|E_{p,m}[\bar{k}]\right|^2 + c}, \quad (31)$$

where $U_{p,m}[\bar{k}]$ and $E_{p,m}[\bar{k}]$ are the m-th element of $\mathbf{U}_p[\bar{k}]$ and $\mathbf{E}_p[\bar{k}]$, respectively and c is a small constant.

The update equations of the PBFD $\hat{\mathbf{F}}_p[\bar{k}]$ are summarized in Table 1. In the simulations, we set $M = 64$, $P = 32$, $\bar{\mu}_m = 0.01$. The block length L is chosen such that the processing delay $2L - 1$ does not exceed the desired total processing delay d_G (e.g., $L = 32$ for $d_G \geq 4$ ms; $L = 8$ for $d_G = 1$ ms; $L = 16$ for $d_G = 2 - 3$ ms).

3.2. Bias of the CAF

The presence of the closed signal loop $G(q,k)$ introduces specific signal correlation when the desired signal $x[k]$ is spectrally colored (e.g., a speech or music signal). As a result, the CAF fails to provide a reliable feedback path estimate [28].

Let us again assume the sufficient-order case where $L_{\hat{F}} = L_F$. Then, the feedback path estimate $\hat{\mathbf{f}}[k]$ can be decomposed as (see (16)):

$$\hat{\mathbf{f}}[k] = \mathbf{f}[k] + \underbrace{\mathcal{E}\{\mathbf{u}[k]\mathbf{u}^T[k]\}^{-1}\mathcal{E}\{\mathbf{u}[k]x[k]\}}_{\text{bias}}. \quad (32)$$

If $\mathcal{E}\{\mathbf{u}[k]x[k]\} = \mathbf{0}$, the feedback path estimate $\hat{\mathbf{f}}[k]$ is unbiased.

However, because of the presence of the forward path $G(q,k)$, the input signal $u[k]$ to the adaptive filter $\hat{\mathbf{f}}[k]$ relates to $x[k]$ as

$$u[k] = C(q,k)x[k], \quad (33)$$

where $C(q,k)$ is defined in (9).

Usually, $G(q,k)$ contains a processing delay d_G of at least one sample[2]. Assuming that $G(q,k)$, $F(q,k)$, and $\hat{F}(q,k)$ are causal, the closed-loop system $C(q,k)$ can be specified as

$$\begin{aligned} C(q,k) &= c_{d_G}[k]q^{-d_G} + c_{d_G+1}[k]q^{-d_G-1} \\ &\quad + \cdots + c_{L_C-1}[k]q^{-L_C+1} \end{aligned} \quad (34)$$

and hence

$$\begin{aligned} u[k] &= (c_{d_G}[k] + \ldots \\ &\quad + c_{L_C-1}[k]q^{-L_C+d_G+1})\, x[k-d_G]. \end{aligned} \quad (35)$$

As a result, $\mathcal{E}\{\mathbf{u}[k]x[k]\} = \mathbf{0}$ if and only if

$$\mathcal{E}\{x[k-\delta]x[k]\} = 0 \quad (36)$$

for $d_G \leq \delta \leq L_C + L_{\hat{F}} - 2$.

Most practical sound signals $x[k]$ are *spectrally colored*, meaning that the signal values $x[k]$ are correlated in time (e.g., speech, music, etc). Many of these audio signals may be well approximated as low-order, time-varying auto-regressive (AR) random processes

$$x[k] = H(q,k)w[k] = \frac{1}{A(q,k)}w[k], \quad (37)$$

where $A(q,k)$ is a Finite Impulse Response (FIR) with $a_0 = 1$ and where $w[k]$ is a white noise signal. Hence, the signal model $H(q)$ is often Infinite Impulse Response (IIR), so that the length L_H of $H(q)$ typically exceeds d_G and hence, $\mathcal{E}\{\mathbf{u}[k]x[k]\} \neq 0$. The CAF will then cancel the desired signal $x[k]$ instead of the feedback signal $n[k] = F(q,k)u[k]$ (see (16)), leading to signal distortion.

From (16), we observe that the bias in the feedback path estimate $\hat{\mathbf{f}}[k]$ decreases with an increasing power ratio of the feedback signal $n[k]$, i.e., the signal to identify, to the desired signal $x[k]$, which acts as a disturbance. Since

$$n[k] = F(q,k)C(q,k)x[k], \quad (38)$$

the larger the loop gain $|G(q,k)F(q,k)|$, the smaller the bias will be. This indicates that the bias will be smallest for large gains $G(q,k)$ and for frequencies that are closest to instability, which is a desirable property.

3.3. Reducing the bias of the CAF

Classical approaches to reduce the bias of the CAF include inserting signal decorrelation operations in the forward path $G(q,k)$ and reducing the adaptation speed of the feedback canceller.

Inserting signal decorrelation operations

A first solution to reduce the bias is to include decorrelating signal operations in cascade with the forward path $G(q,k)$, as depicted in Figure 4. Ideally, the decorrelation unit removes any correlation between the desired signal $x[k]$ and the input $u[k]$ to the adaptive filter $\hat{F}(q,k)$, so that the bias term in (32) equals zero. Often, the decorrelation unit however degrades

[2] Note that the delay d_G includes the processing delay of the DAC and the ADC of the hearing aid (see Section 2).

the sound quality, making full decorrelation impossible.

For many signals $x[k]$, the autocorrelation sequence $\mathcal{E}\{x[k]x[k-\delta]\}$ decreases with increasing lag δ. A common technique to reduce the correlation is to increase the delay d_G by inserting a delay in the forward path [28]. Many audio signals however have a relatively strong autocorrelation. A large delay d_G may then be required to efficiently decorrelate $x[k]$ and $u[k]$. However, the delay d_G should not exceed 10 ms in order not to degrade intelligibility [29] and sound quality, e.g., by comb filter effects resulting from destructive and constructive interference between the direct sound to the eardrum and the amplified and delayed sound [30, 31].

As an illustration, Figure 5 depicts the misalignment of the PBFD CAF as a function of the delay d_G of $G(q,k) = Gq^{-d_G}$ with $G = 10$ dB for the acoustic feedback path in Figure 2 with a mobile phone attached to the head. Three desired signals $x[k]$ are considered: a white noise signal, a stationary speech weighted noise signal and a real speech signal. The real speech signal consists of English sentences spoken by a male speaker from the Hearing in Noise Test (HINT) database [32]. For speech weighted noise and real speech, the CAF is clearly biased. For both signals, the bias (or misalignment) decreases with increasing delay d_G. A delay of 4 ms provides sufficient decorrelation for the speech weighted noise signal. However, for the real speech signal, a much larger delay $d_G > 10$ ms is required.

Other techniques to reduce the correlation between $x[k]$ and $u[k]$ are inserting a probe signal $r[k]$ (noise signal) at the input $u[k]$ of the loudspeaker (see Figure 4) or adding non-linearities to the forward path $G(q,k)$, such as frequency shifting, phase or delay modulation [12, 33, 34, 35]. Such methods may, however, degrade the sound quality. In the former case, e.g., the probe signal should be inaudible so that it does not degrade the signal-to-noise ratio. Its level will thus have to be lower than the level of the ordinary output $u[k]$, resulting in a significant residual bias. A small amount of modulation or a small frequency shift (e.g., a frequency shift up to 5 Hz [13]) may still be acceptable for speech signals, however, its effect on music is objectionable. These techniques will not be further discussed.

Reducing the adaptation speed

In [36, 37, 38], distortion of the desired signal $x[k]$ is reduced by keeping the adaptation speed of the feedback canceller small. When feedback or a sudden change in the feedback path is detected, the adaptation speed is temporarily increased. A slow adaptation speed reduces the ability to track changes in the spectrum of the desired signal $x[k]$, and hence, limits the negative effect of a temporary signal with a strong autocorrelation on the feedback path estimate [30]. Convergence of this technique may however be too slow to successfully track variations in the feedback path so that the maximum amplification may still be limited.

In addition to inserting signal decorrelating operations or reducing the adaptation speed, other approaches have been proposed in the literature for improving the estimation accuracy of the adaptive feedback canceller. A first class of techniques (described in Section 4) exploits prior knowledge of the acoustic feedback path to improve the adaptation of the feedback canceller. A second class of techniques (discussed in Section 5) views the feedback path as a part of a closed-loop system and applies closed-loop system identification theory.

4. FEEDBACK CANCELLATION BASED ON PRIOR KNOWLEDGE OF THE ACOUSTIC FEEDBACK PATH

In [15, 22, 39], prior knowledge of the acoustic feedback path is exploited to reduce the bias of the standard CAF. The adaptation of the feedback canceller is controlled based on the prior knowledge through constrained (Section 4.1) or bandlimited adaptation (Section 4.2).

4.1. Constrained adaptation (C-CAF)

In [22, 39], the bias is reduced by constrained adaptation: the filter coefficients $\hat{\mathbf{f}}[k]$ of the adaptive feedback canceller $\hat{F}(q,k)$ are not allowed to deviate too much from reference filter coefficients $\hat{\mathbf{f}}_{ref}$. These reference filter coefficients $\hat{\mathbf{f}}_{ref}$ are measured during start-up or fitting, by means of a probe signal $r[k]$.

A cheap method to impose this constraint is to add a term to the cost function (12) of the feedback canceller that penalizes excessive deviation of the filter $\hat{\mathbf{f}}[k]$ from the reference filter $\hat{\mathbf{f}}_{ref}$, i.e.,

$$J(\hat{\mathbf{f}}[k]) = \mathcal{E}\{\left|y[k] - \hat{\mathbf{f}}^T[k]\mathbf{u}[k]\right|^2\} + \eta\left(\hat{\mathbf{f}}[k] - \hat{\mathbf{f}}_{ref}\right)^T\left(\hat{\mathbf{f}}[k] - \hat{\mathbf{f}}_{ref}\right). \quad (39)$$

This results in the solution

$$\hat{\mathbf{f}}[k] = \left(\mathcal{E}\{\mathbf{u}[k]\mathbf{u}^T[k]\} + \eta\mathbf{I}\right)^{-1} \cdot \left(\mathcal{E}\{\mathbf{u}[k]y[k]\} + \eta\hat{\mathbf{f}}_{ref}\right). \quad (40)$$

The scalar η trades off between signal distortion reduction and the ability to model deviations from $\hat{\mathbf{f}}_{ref}$. The larger η, the more $\hat{\mathbf{f}}[k]$ evolves towards $\hat{\mathbf{f}}_{ref}$.

Time-domain NLMS

From (39), the following time-domain NLMS update equation can be derived

$$\hat{\mathbf{f}}[k+1] = \hat{\mathbf{f}}[k] + \frac{\bar{\mu}}{L_{\hat{F}}\left(\overline{|u[k]|^2} + \overline{|e[k]|^2}\right) + \eta + c} \cdot \left[\mathbf{u}[k]\left(y[k] - \hat{\mathbf{f}}^T[k]\mathbf{u}[k]\right) - \eta\left(\hat{\mathbf{f}}[k] - \hat{\mathbf{f}}_{ref}\right)\right]. \quad (41)$$

Partitioned-block frequency-domain NLMS

Converting (41) into the partitioned-block frequency-domain, results in [27]:

$$\hat{\mathbf{F}}_p[\bar{k}+1] = \hat{\mathbf{F}}_p[\bar{k}] + \boldsymbol{\Delta}[\bar{k}]\left(\boldsymbol{\mathcal{F}}\mathbf{g}\boldsymbol{\mathcal{F}}^{-1}\mathbf{U}_p^H[\bar{k}]\mathbf{E}[\bar{k}] - \boldsymbol{\eta}(\hat{\mathbf{F}}_p[\bar{k}] - \hat{\mathbf{F}}_{p,ref})\right), \quad (42)$$

where

$$\hat{\mathbf{f}}_{p,ref} = \left[\begin{array}{cccc} \hat{f}_{ref,pP} & \cdots & \hat{f}_{ref,(p+1)P-1} \end{array}\right]^T, \quad (43)$$

$$\hat{\mathbf{F}}_{p,ref} = \boldsymbol{\mathcal{F}}\left[\begin{array}{c} \hat{\mathbf{f}}_{p,ref} \\ \mathbf{0} \end{array}\right]\begin{array}{l}\updownarrow P \\ \updownarrow M-P\end{array}. \quad (44)$$

The matrix $\boldsymbol{\eta}$ is a diagonal matrix that contains the trade-off parameters η_m, $m = 0, \ldots, M-1$ of the different frequency bins m. The diagonal step size matrix $\boldsymbol{\Delta}[\bar{k}]$ equals

$$\boldsymbol{\Delta}[\bar{k}] = \text{diag}\{\mu_0[\bar{k}], \ldots, \mu_{M-1}[\bar{k}]\} \quad (45)$$

with

$$\mu_m[\bar{k}] = \frac{\bar{\mu}_m}{\sum_{p=0}^{\frac{L_{\hat{F}}}{P}-1}\left|U_{p,m}[\bar{k}]\right|^2 + \frac{L_{\hat{F}}}{P}\left|E_{p,m}[\bar{k}]\right|^2 + \eta_m + c} \quad (46)$$

In the sequel, the CAF with constrained adaptation will be referred to as C-CAF.

Performance

Figure 6 illustrates the effect of $\eta_m = \eta$ on the performance of the PBFD C-CAF for different delays d_G and real speech as a desired signal. The reference filter $\hat{\mathbf{f}}_{ref}$ is a 20-taps filter. It was computed for the scenario without obstruction by disconnecting the forward path $G(q,k)$ and inserting a white noise signal $r[k]$ into the loudspeaker. The frequency response of the reference filter $\hat{\mathbf{f}}_{ref}$ together with the frequency response of the true feedback path is depicted in Figure 7. The feedback path when a mobile phone is attached to the ear is also shown. Figure 6(a) shows the misalignment for the feedback path without obstruction. Figure 6(b) depicts the misalignment for the feedback path with a mobile phone attached to the head, illustrating the performance of the C-CAF in the presence of a deviation in the feedback path model. The forward path gain was set close to instability, i.e., $G = 17$ dB for the scenario without obstruction and $G = 10$ dB for the scenario with a mobile phone.

For the scenario without obstruction, the reference filter is a good model of the actual feedback path. As a result, the misalignment of the C-CAF decreases with increasing η. When the mobile phone is attached to the head, the actual feedback path deviates from the reference path (see Figure 6). If η is chosen too large, the feedback path deviation cannot be successfully modelled. Indeed, Figure 6(b) shows that for $\eta = 0.2$, a similar or worse misalignment is obtained than for $\eta = 0.04$. In the sequel, $\eta = 0.04$.

4.2. Bandlimited adaptation (BL-CAF)

In [15, 38, 40, 41, 42], feedback cancellation is restricted to the frequency band that encompasses the unstable frequencies through bandlimited adaptation.

Indeed, to avoid instability, it suffices that the feedback canceller cancels the feedback signal at the critical frequencies, where instability is about to occur. Typically, the acoustic feedback path of a hearing aid provides less attenuation at high frequencies, where most hearing aid users have the largest hearing loss (see Figure 2) [3]. As a result, the risk for instability is often highest in the high frequency range, while most of the desired signal energy is typically concentrated at low frequencies, e.g., for speech signals. By concentrating the adaptation of the feedback canceller on the higher frequencies only, the feedback canceller may be more efficient and will introduce less distortion.

Figure 8 depicts the block diagram of the bandlimited feedback canceller (abbreviated as BL-CAF). The filters $B_1(q)$ and $B_2(q)$ are high or band pass filters chosen such that all critical frequencies are preserved while the desired signal components are removed as much as possible. The filter $B_1(q)$ in the feedback cancellation path limits the feedback cancellation signal to the frequency band of interest and hence, prevents the desired signal components outside the critical band from being distorted by the feedback canceller $\hat{F}(q,k)$. To focus the modeling effort of the adaptive feedback canceller $\hat{\mathbf{f}}[k]$ on the regions that contain the critical frequencies, the adaptive filter minimizes the frequency-weighted error energy

$$\begin{aligned} J(\hat{\mathbf{f}}[k]) &= \mathcal{E}\{\Big|B_2(q)\left(y[k]-\hat{F}(q,k)u^{BP_1}[k]\right)\Big|^2\} \\ &= \mathcal{E}\{\Big|y^f[k]-\hat{F}(q,k)u^f[k]\Big|^2\}, \end{aligned} \quad (47)$$

where

$$u^{BP_1}[k] = B_1(q)u[k], \quad (48)$$

$$y^f[k] = B_2(q)y[k], \quad (49)$$

$$u^f[k] = B_2(q)u^{BP_1}[k]. \quad (50)$$

The filter $B_2(q)$ reduces the energy of the residual error signal (which acts as a disturbance to the adaptive feedback canceller). As a result, the misadjustment and bias of the bandlimited adaptive feedback canceller is reduced compared to the standard CAF.

Note that the filter $B_1(q)$ introduces a group delay in the feedback cancellation path. This group delay should not exceed the delay in the acoustic feedback path, otherwise the feedback signal can not be cancelled [15]. To guarantee a small group delay and to save computational complexity, low-order elliptic IIR filters $B_1(q)$ and $B_2(q)$ are used in [15].

In [15], minimization of (47) is realized through a filtered-X algorithm. In the filtered-X algorithm, the input signal $u^{BP_1}[k]$ and the feedback-compensated signal $e[k] = y[k] - \hat{F}(q,k)u^{BP_1}[k]$ are filtered by $B_2(q)$ before being used to update the adaptive filter $\hat{F}(q,k)$. Equivalently, $J(\mathbf{f}[\hat{\mathbf{k}}])$ can be minimized by performing standard adaptive filtering techniques on the pre-filtered microphone and loudspeaker data $y^f[k]$ and $u^f[k]$ (as is illustrated in Figure 8) [27]. In contrast to the filtered-X algorithm, any change to the adaptive filter $\hat{\mathbf{f}}[k]$ then has an immediate effect on the frequency-weighted adaptation error even if $B_2(q)$ has a group delay. As a result, no stability problems may occur [15, 43].

Time-domain NLMS

For NLMS adaptation, the update equation becomes

$$\hat{\mathbf{f}}[k] = \hat{\mathbf{f}}[k-1] + \mu[k]\mathbf{u}[k]\underbrace{\left(y^f[k]-\hat{\mathbf{f}}^T[k-1]\mathbf{u}^f[k]\right)}_{e^f[k]}, \quad (51)$$

with

$$\mathbf{u}^f[k] = \left[\; u^f[k] \;\; \ldots \;\; u^f[k-L_{\hat{F}}] \;\right] \quad (52)$$

$$\mu[k] = \frac{\bar{\mu}}{L_{\hat{F}}\left(\overline{|u^f[k]|^2}+\overline{|e^f[k]|^2}\right)+c}, \quad (53)$$

Partitioned-block frequency-domain

The PBFD implementation equals [27]

$$\hat{\mathbf{F}}_p[\bar{k}+1] = \hat{\mathbf{F}}_p[\bar{k}] + \boldsymbol{\Delta}[\bar{k}]\boldsymbol{\mathcal{F}}\mathbf{g}\boldsymbol{\mathcal{F}}^{-1}\mathbf{U}_p^{f,H}[\bar{k}]\mathbf{E}^f[\bar{k}], \quad (54)$$

where

$$\mathbf{U}_p^f[\bar{k}] = \text{diag}\left\{\boldsymbol{\mathcal{F}}\begin{bmatrix} u^f[(\bar{k}+1)L-pP-M+1] \\ \vdots \\ u^f[(\bar{k}+1)L-pP] \end{bmatrix}\right\}, \quad (55)$$

$$\mathbf{E}^f[\bar{k}] = \boldsymbol{\mathcal{F}}\begin{bmatrix} \mathbf{0} \\ \mathbf{I}_L \end{bmatrix}\Big(\mathbf{y}_{\bar{k}}^f - \begin{bmatrix} \mathbf{0} & \mathbf{I}_L \end{bmatrix}\boldsymbol{\mathcal{F}}^{-1}\sum_{p=0}^{\frac{L_{\hat{F}}}{P}-1}\mathbf{U}_p^f[\bar{k}]\hat{\mathbf{F}}_p[\bar{k}]\Big), \quad (56)$$

$$\mathbf{y}_{\bar{k}}^f = \begin{bmatrix} y[\bar{k}L+1] & \dots & y[(\bar{k}+1)L] \end{bmatrix}^T. \quad (57)$$

The step sizes $\mu_m[\bar{k}]$ are computed as:

$$\frac{\bar{\mu}_m}{\sum_{p=0}^{\frac{L_{\hat{F}}}{P}-1}\left|U_{p,m}^f[\bar{k}]\right|^2 + \frac{L_{\hat{F}}}{P}\left|E_{p,m}^f[\bar{k}]\right|^2 + c}. \quad (58)$$

Performance

The bandwidths and the stopband attenuation of the filters $B_1(q)$ and $B_2(q)$ determine the efficiency of the bandlimited feedback canceller $\hat{F}(q,k)$: The larger the bandwidth (or the smaller the stopband attenuation), the larger the frequency range where acoustic feedback is cancelled, but the larger the bias and misadjustment of the feedback path estimate. To specify the bandwidth of $B_1(q)$ and $B_2(q)$, identification of the critical frequency region for different hearing aids and different hearing aid users is required, e.g., during fitting. However, the critical frequency region expands with increasing gain in the forward path $G(q,k)$ as well as, e.g., with the presence of a telephone handset or hand palm close to the ear (see Figure 2). Hence, to guarantee stability, the bandwidth and stopband attenuation of $B_1(q)$ and $B_2(q)$ should not be chosen too small. In this chapter, a second-order IIR filter $B_1(q) = B_2(q)$ with a cut-off frequency of 1 kHz and a stopband attenuation of 20 dB is used.

As an illustration, Figure 9 depicts the misalignment of the BL-CAF as a function of the forward path delay d_G for three different cut-off frequencies f_c, i.e., $f_c = 0.4$ kHz, $f_c = 1$ kHz and $f_c = 2$ kHz. For comparison, the misalignment of the CAF is also shown. The acoustic feedback path with a mobile phone attached to the head is used. The desired signal $x[k]$ is a real speech signal. Two forward path gains G are depicted, i..e, $G = 10$ dB and $G = 17$ dB. For all delays d_G, the BL-CAF achieves a smaller misalignment than the CAF, especially for low gains G. For $G = 10$ dB, a cut-off frequency of 1 kHz and 2 kHz results in a smaller misalignment than a cut-off frequency of 0.5 kHz. For $G = 17$ dB, the cut-off frequency of 2 kHz performs worse than $f_c = 1$ kHz: for $d_G \geq 5$ ms, instability even occurs. At high gains, the region with critical frequencies increases, explaining the worse performance. This illustrates that f_c should not be chosen too large.

5. FEEDBACK CANCELLATION BASED ON CLOSED-LOOP SYSTEM IDENTIFICATION

All of the above mentioned feedback cancellation techniques initially ignore the presence of the closed signal loop $G(q,k)$ and apply the standard adaptive filtering techniques for open-loop systems. In a second stage, signal processing operations are included to reduce the negative effect of $G(q,k)$ on the performance.

An alternative approach is to immediately view the feedback path as a part of a closed-loop system and to apply closed-loop system identification theory [1, 17, 30, 44, 45]. Closed-loop identification methods can be classified as direct, indirect or joint input-output methods [1]. In contrast to the indirect and the joint input-output approach, the direct method requires neither assumptions about the forward path $G(q,k)$ (e.g., linear) nor the presence of an external probe signal $r[k]$, making it an appealing approach for feedback cancellation.

Section 5.1 defines the closed-loop system set-up. Section 5.2 describes the direct method of closed-loop system identification in the context of feedback cancellation. In this method, the bias of the standard CAF is reduced by incorporating a (stationary or time-varying) model of the desired signal $x[k]$ in the identification [18, 30, 45, 46]. The estimation of the desired signal model is discussed in Section 5.3. Section 5.4 discusses the other two closed-loop system identification procedures, i.e., the indirect method and the joint input-output method [17, 47].

5.1. Closed-loop system set-up

Figure 10 depicts the closed-loop system set-up. The *open-loop system to be identified* is given by

$$y[k] = F(q,k)u[k] + x[k]. \quad (59)$$

For the time being, we assume that the desired signal $x[k]$ can be modelled as

$$x[k] = H(q,k)w[k], \quad (60)$$

with $w[k]$ a zero mean, white noise sequence and $H(q,k)$ monic and inversely stable.

The output signal $y[k]$ is fed-back to the input $u[k]$ according to

$$u[k] = G(q,k)\left(y[k] - \hat{F}(q,k)u[k]\right) + r[k] \quad (61)$$

The signal $r[k]$ is an optional probe signal that is independent of $x[k]$, and can be viewed as an extra excitation signal of the feedback path $F(q,k)$. The probe signal is generally a noise signal.

By combining (59) and (61), we obtain the closed-loop relations [1, 44]

$$\begin{aligned} y[k] &= (1 + F(q,k)C(q,k))\,x[k] \\ &\quad + F(q,k)S(q,k)r[k], \quad (62) \\ u[k] &= C(q,k)x[k] + S(q,k)r[k], \quad (63) \end{aligned}$$

where $S(q,k)$ is the so-called sensitivity function

$$S(q,k) = \frac{1}{1 - G(q,k)\left(F(q,k) - \hat{F}(q,k)\right)} \quad (64)$$

and $C(q,k)$ is the closed-loop transfer function from $x[k]$ to $u[k]$ (see (9) in Section 2)

$$C(q,k) = S(q,k)G(q,k). \quad (65)$$

For future use, we denote the closed-loop transfer function from $r[k]$ to $y[k]$ as $F^c(q,k)$:

$$F^c(q,k) = F(q,k)S(q,k). \quad (66)$$

Depending on the assumptions that are made about the forward path $G(q,k)$, closed-loop identification methods can be classified as *indirect, joint input-output* or *direct* methods [1, 44].

5.2. Direct method

In the direct method of closed-loop identification, the open-loop system $\{F(q,k),\ H(q,k)\}$

$$y[k] = F(q,k)u[k] + H(q,k)w[k], \quad (67)$$

is identified from the loudspeaker signal $u[k]$ and the microphone signal $y[k]$ by an open-loop identification method, thereby ignoring the presence of the closed signal loop $G(q,k)$ [18, 30, 45, 48]. Only some specific open-loop identification methods can be applied to closed-loop systems, such as the prediction error method (PEM) [1, 44]. The PEM produces an estimate $\hat{F}(q,k)$ and $\hat{H}(q,k)$ of the feedback path $F(q,k)$ and the desired signal model $H(q,k)$, respectively, by minimizing the energy of the so-called prediction error

$$e^p[k] = \hat{H}(q,k)^{-1}\left(y[k] - \hat{F}(q,k)u[k]\right),$$

i.e,

$$\begin{aligned} J(\hat{\mathbf{f}}[k]) &= \mathcal{E}\{\left|\hat{H}(q,k)^{-1}\Big(y[k] - \hat{F}(q,k)u[k]\Big)\right|^2\}, \\ &= \mathcal{E}\{\left|y^f[k] - \hat{\mathbf{f}}^T[k]\mathbf{u}^f[k]\right|^2\}, \quad (68) \end{aligned}$$

where

$$\mathbf{u}^f[k] = \left[\ u^f[k]\ \ \ldots\ \ u^f[k - L_{\hat{F}} + 1]\ \right]^T, \quad (69)$$

$$\begin{aligned} y^f[k] &= \hat{H}(q,k)^{-1}y[k] \quad (70) \\ u^f[k] &= \hat{H}(q,k)^{-1}u[k]. \quad (71) \end{aligned}$$

Minimization of (68) results in

$$\hat{\mathbf{f}}[k] = \mathcal{E}\{\mathbf{u}^f[k]\mathbf{u}^{f,T}[k]\}^{-1}\mathcal{E}\{\mathbf{u}^f[k]y^f[k]\}, \quad (72)$$

where $y^f[k]$ can be decomposed as:

$$y^f[k] = \hat{H}(q,k)^{-1}x[k] + F(q,k)u^f[k]. \quad (73)$$

If $\hat{H}(q,k) = H(q,k)$

$$y^f[k] = w[k] + F(q,k)u^f[k]. \quad (74)$$

The desired signal $x[k]$ is converted in a white noise signal $w[k]$. As a result, $\hat{\mathbf{f}}[k]$ results in an unbiased

feedback path estimate in the sufficient order case (i.e., $L_{\hat{F}} = L_F$) [18, 45].

From (68) it follows that $J(\hat{\mathbf{f}}[k])$ can be minimized by performing standard adaptive filtering techniques on the pre-whitened data $y^f[k]$ and $u^f[k]$ [43]. This is illustrated in Figure 11, where $A(q,k) = \hat{H}(q,k)^{-1}$. The update equations of the time-domain and PBFD NLMS algorithm correspond to (51)-(58) with now $y^f[k]$ and $u^f[k]$ defined in (70)-(71) (see Table 2). In the sequel, we refer to the feedback canceller based on the PEM as PEMAFC.

5.3. Desired signal model

The PEMAFC requires an estimate of the desired signal model $H(q,k)$. Both, fixed and adaptive estimates of the desired signal model $H^{-1}(q,k)$ have been considered in the literature. In the sequel, the PEMAFC with fixed model is referred to as PEMAFC-f and the PEMAFC with adaptive model is referred to as PEMAFC-a.

Fixed desired signal model (PEMAFC-f)

In [30, 45], the desired signal model $H(q,k)$ is approximated by a *fixed* low pass all-pole filter $\hat{H}(q,k) = A^{-1}(q)$, which represents the long-term average speech spectrum. A simple model for the average speech spectrum is a first-order all-pole model:

$$\hat{H}(q,k) = \frac{1}{1-\alpha q^{-1}}, \tag{75}$$

with $\alpha < 1$ (e.g., $\alpha = 0.9$) [22].

Adaptive desired signal model (PEMAFC-a)

In practice, the desired signal model $H^{-1}(q,k)$ is unknown and highly time-varying. In addition, the quality of the feedback canceller $\hat{F}(q,k)$ strongly depends on the accuracy of the signal model estimate $\hat{H}(q,k)$ [45], so that it is desirable to identify the feedback path $F(q,k)$ as well as the desired signal model $H(q,k)$ with the PEM method. However, $F(q,k)$ and $H(q,k)$ are not always identifiable in the closed-loop system at hand [45].

Since most audio signals $x[k]$ can be approximated by a low-order AR model, it is assumed that

$$H^{-1}(q,k) = A(q,k) = 1 + q^{-1}\bar{A}(q,k) \tag{76}$$

with $\bar{A}(q,k)$ an FIR filter. In [18], it has been shown that the AR model $A(q,k)$ and the feedback path $F(q,k)$ can be both identified in closed-loop without adding non-linearities or a probe signal, if the delay $d_G \geq L_{H^{-1}} = L_A$.

Since the filter length L_A is short, the required processing delay d_G is usually much shorter (e.g., 1-2 ms) than the delay d_G that is needed in the standard CAF to decorrelate $x[k]$ and $u[k]$. For example, a 10-20 ms speech segment at a sampling frequency $f_s = 16$ kHz can be modelled by a 10-20th order AR model with $w[k]$ a white noise excitation (in case of unvoiced sounds) or a pulse train excitation (in case of voiced sounds).

The AR model $A(q,k)$ is computed through linear prediction of the feedback compensated signal

$$e[k] = y[k] - \hat{\mathbf{f}}^T[k]\mathbf{u}[k], \tag{77}$$

on subsequent frames of $N = 160$ samples (i.e., 10 ms), e.g., using the Levinson-Durbin algorithm [49]. Note that $e[k] = x[k]$, if $\hat{\mathbf{f}}[k] = \mathbf{f}[k]$.

So far, we have assumed that the excitation $w[k]$ of $H(q,k)$ is a white noise sequence. This assumption does not apply for voiced speech, where the excitation $w[k]$ approximates a pulse train that is periodical with the pitch period P (expressed as number of samples). A low-order (e.g., $10-20$th order) AR model will not suffice to notch out the discrete frequencies caused by the pulse train excitation. As a result, the pre-filtered loudspeaker signal $u^f[k]$ will still be correlated with the excitation signal $w[k]$ at the pitch frequency $\frac{f_s}{P}$ and its harmonics $k\frac{f_s}{P}$ with $k \in \mathbb{N}$ and $\frac{k}{P} < \frac{1}{2}$. The residual correlation caused by the pulse train excitation can be removed by cascading the low-order short-term AR-model $A_{ST}(q,k)$ with a long-term predictor $A_{LT}(q,k) = (1 - bq^{-\hat{P}[k]})$, where $\hat{P}[k]$ is an estimate of the pitch period P [48]:

$$A(q,k) = A_{ST}(q,k)(1 - bq^{-\hat{P}[k]}). \tag{78}$$

For speech, the pitch frequency f_s/P lies between 50 and 400 Hz and hence, for $f_s = 16$ kHz, P lies

between 40 and 320 samples. To guarantee identifiability, the total filter length $\hat{P}[k] + L_{A_{ST}}$of $A(q,k)$ should not exceed the maximum allowable processing delay d_G.

For feedback cancellers $\hat{F}(q,k)$ with a short filter length $L_{\hat{F}} \leq P$ and for small delays d_G, the bias in the feedback path estimate due to the periodic pulse train excitation $w[k]$ is negligible [27]. In hearing aids, the dominant part of the feedback path $F(q,k)$ is quite short, so that a relatively short filter length $L_{\hat{F}}$ is typically used, i.e., $L_{\hat{F}} \leq 100$ [14]. In addition, the delay d_G should be kept small (i.e., ≤ 10 ms). As a result, the benefit of a long-term predictor is limited for hearing aid applications.

The equations of the PBFD NLMS implementation of the PEMAFC-a are summarized in Table 2.

Performance

As an illustration, Figure 12 depicts the misalignment of PEMAFC-f (with the fixed AR model (75)) and PEMAFC-a (with[3] $L_A = 21$) as a function of the delay d_G for the acoustic feedback path with a mobile phone attached to the head and a forward path delay $G = 10$ dB. For comparison, the misalignment of the CAF is also shown.

In Figure 12(a), the desired signal $x[k]$ is speech weighted noise, generated by passing white noise through a 20th order all-pole model. In this example, the desired signal $x[k]$ can be perfectly whitened by a 20th order AR model $A(q,k)$, since the white noise assumption is satisfied and $L_{H^{-1}} = 21$. Indeed, for $d_G \leq 2$ ms, the PEMAFC succeeds to fully decorrelate $x[k]$ and $u[k]$: the same misalignment is obtained as for the CAF with white noise as a desired signal $x[k]$ (see Figure 5)[4]. The fixed all-pole model in the PEMAFC-f whitens the desired signal to some extent such that a better performance is achieved than the CAF. For $d_G \geq 4$ ms, $x[k]$ and $u[k]$ are uncorrelated so that all methods achieve a similar performance.

In Figure 12(b), $x[k]$ is a real speech signal (i.e., male sentences from the HINT database [32]). The model assumptions for $x[k]$ (i.e., the assumption of a AR-model for $H^{-1}(q,k)$ and white noise for $w[k]$) are not completely satisfied, explaining the residual bias. However, for all delays $d_G \leq 10$ ms, the PEMAFC-f and PEMAFC-a achieve a better performance than the CAF. The PEMAFC-a outperforms the PEMAFC-f thanks to the adaptive AR model.

[3] To guarantee identifiability, $L_A = 16$ for $d_G = 1$ ms.

[4] For $d_G = 16$ ms, the AR model is undermodelled (since $L_A = 16$), explaining the worse performance.

5.4. Indirect and joint input-output method

In contrast to the direct method, the indirect and joint input-output method both require the use of a probe signal $r[k]$.

Indirect method

In addition to the use of a probe signal $r[k]$, the indirect method [1, 44] requires knowledge of the forward path $G(q,k)$. This makes it not very suitable for hearing aids because $G(q,k)$ often contains user-dependent and adaptive signal processing features, e.g., dynamic range compression.

In the indirect method, the closed-loop transfer function $F^c(q,k)$ (see (66)) from $r[k]$ to $y[k]$ is estimated by means of an adaptive filter $\hat{F}^c(q,k)$. If the forward path $G(q,k)$ is known, the feedback path estimate $\hat{F}(q,k)$ can then be extracted from this closed-loop transfer function estimate $\hat{F}^c(q,k)$. In [50, 51], the estimate of the closed-loop transfer function $F^c(q,k)$ is used as an approximation of $F(q,k)$ i.e., the sensitivity function $S(q,k)$ is assumed to be one. This generally results in a biased feedback path estimate $\hat{F}(q,k)$, especially close to or at instability. In [52], it is shown that the first L_F coefficients of $F^c(q,k)$ are equal to the coefficients of $F(q,k)$ if the forward path delay $d_G \geq L_{\hat{F}}$. For a white noise signal $r[k]$ and $L_{\hat{F}} = L_F$, the estimate $\hat{F}^c(q,k)$ is then unbiased.

The identification of the closed-loop system $F^c(q,k)$ is seriously degraded by the presence of the desired signal $x[k]$ (see (62)). As a result, a large noise level or a slow adaptation speed is required to obtain an accurate estimate $\hat{F}^c(q,k)$ (i.e., with a small variance).

Joint input-output method

In [47], the joint input-output method is applied to obtain an unbiased feedback path estimate $\hat{F}(q,k)$.

In this approach, the forward path $G(q,k)$ is assumed to have a certain structure (e.g., a linear filter) and the microphone signal $y[k]$ and the loudspeaker signal $u[k]$ are jointly viewed as the output of a system driven by the probe signal $r[k]$ (see (62)-(63)) [1, 44]:

$$\begin{bmatrix} y[k] \\ u[k] \end{bmatrix} = \begin{bmatrix} F^c(q,k) \\ S(q,k) \end{bmatrix} r[k] + \begin{bmatrix} 1 + F(q,k)C(q,k) \\ C(q,k) \end{bmatrix} x[k]. \tag{79}$$

The closed-loop transfer function $F^c(q,k)$ and the sensitivity function $S(q,k)$ are determined by means of standard adaptive filtering techniques performed on the excitation signal $r[k]$. The feedback path estimate $\hat{F}(q,k)$ is then derived from these two model estimates $\hat{F}^c(q,k)$ and $\hat{S}(q,k)$ as:

$$\hat{F}(q,k) = \hat{F}^c(q,k)\hat{S}^{-1}(q,k). \tag{80}$$

In [47], $\hat{F}(q,k)$ is realized as an adaptive FIR filter that minimizes the error energy

$$\mathcal{E}\{\left|\hat{F}^c(q,k)r[k] - \hat{F}(q,k)\hat{S}(q,k)r[k]\right|^2\}. \tag{81}$$

In [17], the feedback path $F(q,k)$ is identified with a two-stage method, requiring only two adaptive filters. In a first stage, the sensitivity function $S(q,k)$ from $r[k]$ to $u[k]$ is determined using a standard adaptive filter. The output $z_1[k] = \hat{S}(q,k)r[k]$ of the first adaptive filter is then fed to the input of a second adaptive filter $\hat{F}(q,k)$ that minimizes

$$\mathcal{E}\{\left|y[k] - \hat{F}(q)z_1[k]\right|^2\}. \tag{82}$$

Both implementations require the use of an external identification signal $r[k]$. The identification of $F^c(q,k)$, $S(q,k)$ and $F(q,k)$ is impeded by the presence of the desired signal $x[k]$. To preserve sound quality, the level of the probe signal $r[k]$ should be low with respect to the desired output $G(q)x[k]$. To avoid a large variance in the feedback path estimate, a slow adaptation speed should be used for the adaptive filters [47], at the expense of a poor tracking performance. In addition, large filter lengths are required to accurately identify the closed-loop transfer functions $\hat{F}^c(q,k)$ and $\hat{S}(q,k)$, as they can easily contain narrowband peaks when the closed-loop system $F^c(q,k)$ is close to instability (e.g., for high forward path gains).

6. COMPARISON

This section compares the performance of different adaptive feedback cancellation techniques. We concentrate on the techniques that do not require the use of an external probe signal $r[k]$ during adaptation, i.e., the CAF, the C-CAF, the BL-CAF and the PEMAFC (with fixed and adaptive AR model).

6.1. Steady-state performance

Figure 13 compares the steady-state performance, i.e., the misalignment upon convergence, of the C-CAF ($\eta = 0.04$), BL-CAF, PEMAFC-f and PEMAFC-a for the acoustic feedback path with a mobile phone attached to the head and real speech as a desired signal $x[k]$. The forward path gain equals 10 dB. Figure 13(a) depicts the misalignment of the CAF, the C-CAF and the BL-CAF as a function of the delay d_G; Figure 13(b) compares the misalignment of the CAF, the PEMAFC-f and the PEMAFC-a. For all delays $d_G \in [1, 10]$ ms, the C-CAF, the BL-CAF and the PEMAFC achieve a smaller misalignment than the CAF: depending on the delay d_G and the algorithm, a reduction in misalignment of 1 to 8.5 dB is achieved. The PEMAFC-a generally achieves the best performance.The PEMAFC-f performs 1-2 dB worse than the PEMAFC-a. For delays $d_G > 3$ ms, the BL-CAF and PEMAFC-a have about the same steady-state misalignment.

6.2. Tracking performance

To illustrate the convergence and tracking performance of the algorithms, an abrupt change of the feedback path was simulated after 10 s by switching the test condition from the scenario without obstruction to the scenario with a mobile phone attached to the head. After 20 s the mobile phone was removed again. The forward path gain and delay are $G = 17$ dB and $d_G = 4$ ms. Figure 14(a) depicts the misalignment of the CAF, the C-CAF and the BL-CAF as a function of time; Figure 14(b) depicts the misalignment of the CAF, the PEMAFC-f and the PEMAFC-a.

When the sudden changes in feedback path occur, the hearing aid system temporarily becomes unstable. For this scenario, all algorithms succeed to

re-stabilize the hearing aid after the feedback path changes. The faster the convergence of the algorithm, the shorter the duration of instability. Before 10 s and after 20 s, the C-CAF and BL-CAF converge faster than the CAF and have a smaller misalignment. Between 10 s and 20 s, the CAF performs quite well. During this time period, the loop gain and hence, the energy ratio of the feedback signal to the (disturbing) desired signal is high, explaining the good performance. The PEMAFC methods pre-whiten the desired signal (which acts as a disturbance) to some extent, generally resulting in a faster convergence and hence, better tracking compared to the CAF, the C-CAF and the BL-CAF. Among all algorithms, the PEMAFC-a has the fastest convergence and best tracking performance thanks to the adaptive pre-whitening of the desired signal.

6.3. Measurement of actual maximum stable gain

To illustrate the effective benefit of the different algorithms for a hearing aid user, the MSG of the algorithms was determined by increasing the forward path gain until audible distortion[5] (such as howling) occurred. The desired signal $x[k]$ is a real speech signal, consisting of sentences spoken by a male speaker. The initial gain in the forward path was set at 6 dB below the stability margin. After 1s of convergence, the gain was gradually and slowly increased in steps of 0.1 dB each 0.5 s, while the adaptive algorithm was running.

Table 3 compares the MSG without feedback cancellation (abbreviated in Table 3 as No FC) with the MSG that was achieved with the different algorithms. Three forward path delays d_G are considered, i.e., $d_G = 2$ ms, $d_G = 4$ ms and $d_G = 6$ ms. For $d_G = 2$ ms, the benefit in MSG by the CAF is small: without obstruction, the MSG even decreases. Increasing the delay d_G significantly improves the performance of the CAF (see Figure 5). Indeed, for $d_G = 4$ ms and 6 ms, the CAF on average increases the MSG of the hearing aid by 13.5 dB (without obstruction) and 19.5 dB (with a mobile phone).

For the scenario without obstruction, the C-CAF increases the MSG of the hearing aid by 15 dB. Especially for $d_G = 2$ ms, the C-CAF outperforms the CAF. For the scenario with a mobile phone, the C-CAF does not achieve a better performance than the CAF. For this scenario, the reference filter in the C-CAF significantly deviates from the true feedback path (see Figure 7), explaining the worse performance. The BL-CAF improves the MSG of the hearing aid by 14 dB (without obstruction) and 11 dB (with a mobile phone). For $G > 30$ dB, the frequencies below the cut-off frequency $f_c = 1$ kHz become critical. This explains why the MSG of the BL-CAF with $f_c = 1$ kHz is limited to about 30 dB. The PEMAFC-f and PEMAFC-a increase the MSG of the hearing aid by 17 dB and 22 dB, respectively, for the scenario without obstruction and by 27 dB and 29 dB, respectively, for the scenario with a mobile phone. For all three delays, they outperform the CAF. The PEMAFC-a especially offers a benefit compared to the PEMAFC-f for low delays d_G.

[5] This gain was smaller than the gain at which instability occurred.

7. CONCLUSIONS

This chapter gave an overview of existing feedforward suppression and, in particular, feedback cancellation techniques. The most promising approach to reduce acoustic feedback is the use of a continuous adaptation feedback (CAF) canceller. However, the standard continuous adaptation feedback cancellers (CAF) fail to provide a reliable feedback path estimate, when the desired signal is spectrally colored.

Existing techniques to reduce the bias of the standard CAF were discussed. Common approaches include introducing signal decorrelating operations in the forward path or reducing the adaptation speed of the feedback canceller. Other techniques control the adaptation of the feedback canceller based on prior knowledge of the acoustic feedback path through constrained (C-CAF) or bandlimited adaptation (BL-CAF). A final class of techniques views the feedback path as a part of a closed-loop system and applies closed-loop system identification with the direct method, the indirect method or the joint input-output method. Especially the direct method seems appealing for feedback cancellation, since it does neither rely on any assumptions about the forward path nor on the use of an external excitation signal. In this method, the bias is reduced by incorporating a stationary (PEMAFC-f) or a time-varying (PEMAFC-a) model of the desired signal.

The performance of the CAF, the C-CAF, the BL-CAF and PEMAFC was compared for real speech as a desired signal based on acoustic feedback paths measured in a commercial hearing aid. Simulations showed that the C-CAF, the BL-CAF and PEMAFC all reduce the bias of the CAF, especially for small processing delays. Among all methods, the PEMAFC with adaptive desired signal model (PEMAFC-a) achieved the best tracking performance and largest maximum stable gain.

8. REFERENCES

[1] U. Forssell, *Closed-loop identification - methods, theory and applications*, Ph.D. thesis, Linköping Universitet, Linköping, Sweden, 1999.

[2] L. Ljung and T. Söderström, *Theory and Practice of Recursive Identification.*, MIT Press, Cambridge, MA, 1983.

[3] J. Hellgren, T. Lunner, and S. Arlinger, "System identification of feedback in hearing aids," *Journal of the Acoustical Society of America*, vol. 105, no. 6, pp. 3481–3496, June 1999.

[4] J. Hellgren, T. Lunner, and S. Arlinger, "Variations in the feedback of hearing aids," *Journal of the Acoustical Society of America*, vol. 106, no. 5, pp. 2821–2833, Nov. 1999.

[5] B. Rafaely, M. Roccasalva-Firenze, and E. Payne, "Feedback path variability modeling for robust hearing aids," *Journal of the Acoustical Society of America*, vol. 107, no. 5, pp. 2665–2673, May 2000.

[6] M. R. Stinson and G. A. Daigle, "Effect of handset proximity on hearing aid feedback," *Journal of the Acoustical Society of America*, vol. 115, no. 3, pp. 1147–1156, Mar. 2004.

[7] D. K. Bustamante, T. L. Worrall, and M. J. Williamson, "Measurement and adaptive suppression of acoustic feedback in hearing aids," in *Proc. IEEE Int. Conf. Acoustics, Speech, and Signal Processing (ICASSP)*, Glasgow, Scotland, May 1989, vol. 3, pp. 2017–2020.

[8] V. Hohmann, V. Hamacher, I. Holube, B. Kollmeier, and T. Wittkop, "Method for the operation of a hearing aid device or hearing device system as well as hearing aid device or hearing aid device system," U.S. patent, US 2002/0176595 A1, 2002.

[9] J. A. Maxwell and P. M. Zurek, "Reducing acoustic feedback in hearing aids," *IEEE Trans. Speech, Audio Processing*, vol. 3, no. 4, pp. 304–313, July 1995.

[10] R. Porayath and J. Daniel, "Acoustic feedback elimination using adaptive notch filter algorithm," U.S. patent, US 5999631, 1999.

[11] R. Wang and R. Harjani, "Acoustic feedback cancellation in hearing aids," in *Proc. IEEE Int. Conf. Acoustics, Speech, and Signal Processing (ICASSP)*, Minneapolis, USA, Apr. 1993, vol. 1, pp. 137–140.

[12] J. L. Nielsen and U. P. Svensson, "Performance of some linear time-varying systems in control of acoustic feedback," *Journal of the Acoustical Society of America*, vol. 1, no. 106, pp. 240–254, July 1999.

[13] M. R. Schroeder, "Improvement of acoustic-feedback stability by frequency shifting," *Journal of the Acoustical Society of America*, vol. 36, no. 9, pp. 1718–1724, Sept. 1976.

[14] J. M. Kates, "Room reverberation effects in hearing aid feedback cancellation," *Journal of the Acoustical Society of America*, vol. 109, no. 1, pp. 367–378, Jan. 2001.

[15] H.-F. Chi, S. X. Goa, S. D. Soli, and A. Alwan, "Band-limited feedback cancellation with a modified filtered-X LMS algorithm for hearing aids," *Speech Communication*, vol. 39, no. 1-2, pp. 147–161, Jan. 2003.

[16] J. E. Greenberg, P. M. Zurek, and M. Brantley, "Evaluation of feedback-reduction algorithms for hearing aids," *Journal of the Acoustical Society of America*, vol. 108, no. 5, pp. 2366–2376, Nov. 2000.

[17] N. A. Shusina and B. Rafaely, "Unbiased adaptive feedback cancellation in hearing aids by closed-loop identification," *IEEE Trans. Audio, Speech, and Language Processing*, vol. 14, no. 2, pp. 658–665, Mar. 2006.

[18] A. Spriet, I. Proudler, M. Moonen, and J. Wouters, "Adaptive feedback cancellation in hearing aids with linear prediction of the desired signal," *IEEE Transactions on Signal Processing*, vol. 53, no. 10 (part 1), pp. 3749–3763,

Oct. 2005.

[19] J. M. Kates, "Feedback cancellation in hearing aids: Results from a computer simulation," *Signal Processing*, vol. 39, no. 3, pp. 553–562, Mar. 1991.

[20] Y. Park, D. Kim, and I. Kim, "An efficient feedback cancellation for multiband compression hearing aids," in *Proc. of 20th Annual Int. Conf. Eng. in Medicine and Biology Soc.*, 1998, vol. 5, pp. 2706–2709.

[21] S. Thipphayathetthana and C. Chinrungrueng, "Variable step-size of the least-mean-square algorithm for reducing acoustic feedback in hearing aids," in *IEEE Asi-Pacific Conf. on Circuits and Systems*, 2000, pp. 407–410.

[22] J. M. Kates, *Adaptive feedback cancellation in hearing aids*, chapter 2 in "Adaptive signal processing: Applications to real-world problems" (Benesty, J. and Huang, Y.), pp. 23–55, Springer-Verlag, 2003.

[23] J. E. Greenberg, "Modified LMS algorithms for speech processing with an adaptive noise canceller," *IEEE Trans. Speech, Audio Processing*, vol. 6, no. 4, pp. 338–350, July 1998.

[24] T. Fillon and J. Prado, "Acoustic feedback cancellation for hearing-aids, using multi-delay filter," in *5th Nordic Signal Processing Symposium (NORSIG)*, on board Hurtigruten, Norway, Oct. 2002.

[25] A. Kaelin, A. Lindgren, and S. Wyrsch, "A digital frequency-domain implementation of a very high gain hearing aid with compensation for recruitment of loudness and acoustic echo cancellation," *Signal Processing*, vol. 64, no. 1, pp. 71–85, 1998.

[26] J.-S. Soo and K. Pang, "Multidelay block frequency domain adaptive filter," *IEEE Trans. Acoust., Speech, and Signal Processing*, vol. 38, no. 4, pp. 788–798, July 1990.

[27] A. Spriet, G. Rombouts, M. Moonen, and J. Wouters, "Adaptive feedback cancellation in hearing aids," *Journal of the Franklin Institute*, vol. 343, p. 545-573, Sept. 2006.

[28] M. G. Siqueira and A. Alwan, "Steady-state analysis of continuous adaptation in acoustic feedback reduction systems for hearing-aids," *IEEE Trans. Speech, Audio Processing*, vol. 8, no. 4, pp. 443–453, July 2000.

[29] M. A. Stone and B. C. J. Moore, "Tolerable hearing aid delays. I. estimation of limits imposed by the auditory path alone using simulated hearing losses," *Ear and Hearing*, vol. 20, no. 3, pp. 182–191, 1999.

[30] J. Hellgren, "Analysis of feedback cancellation in hearing aids with filtered-X LMS and the direct method of closed loop identification," *IEEE Trans. Speech, Audio Processing*, vol. 10, no. 2, pp. 119–131, Feb. 2002.

[31] S. Laugesen, K. V. Hansen, and J. Hellgren, "Acceptable delays in hearing aids and implications for feedback cancellation," *Journal of the Acoustical Society of America*, vol. 105, no. 2, pp. 1211–1212, 1999.

[32] M. Nilsson, S. D. Soli, and A. Sullivan, "Development of the Hearing in Noise Test for the measurement of speech reception thresholds in quiet and in noise," *Journal of the Acoustical Society of America*, vol. 95, no. 2, pp. 1085–1099, Feb. 1994.

[33] A. M. Engebretson and M. F. George, "Properties of an adaptive feedback equalization algorithm," *Journal of Rehabilitation Research and Development*, vol. 30, no. 1, pp. 8–16, 1993.

[34] C. P. Janse and P. A. A. Timmermans, "Signal amplifier system with improved echo cancellation," U.S. patent, US 5748751, 1998.

[35] H. A. L. Joson, F. Asano, Y. Suzuki, and S. Toshio, "Adaptive feedback cancellation with frequency compression for hearing aids," *Journal of the Acoustical Society of America*, vol. 94, no. 6, pp. 3248–3254, Dec. 1993.

[36] T. Kaulberg, "A hearing aid with an adaptive filter for suppression of acoustic feedback," European patent, EP 1191814, 2002.

[37] J. Nielsen and M. Ekelid, "Feedback cancellation using bandwidth detection," WO Patent, WO 01/06746 A2, 2001.

[38] J. Nielsen and M. Ekelid, "Feedback cancellation with low frequency input," WO Patent, WO 01/06812 A1, 2001.

[39] J. M. Kates, "Constrained adaptation for feedback cancellation in hearing aids," *Journal of the Acoustical Society of America*, vol. 106, no. 2, pp. 1010–1019, Aug. 1999.

[40] S. Gao, S. Soli, and H.-F. Chi, "Band-limited adaptive feedback canceller for hearing aids," European patent, EP 1118247, 1999.

[41] B. Rafaely, N. A. Shusina, and J. L. Hayes, "Robust compensation with adaptive feedback cancellation in hearing aids," *Speech Communication*, vol. 39, no. 1-2, pp. 163–170, Jan. 2003.

[42] S. D. Soli, P. Widin, and K. M. Buckley, "Auditory prosthesis, noise suppression apparatus and feedback suppression apparatus having focused adaptive filtering," U.S. patent, US 5402496, 1993.

[43] A. Spriet, I. Proudler, M. Moonen, and J. Wouters, "An instrumental variable method for adaptive feedback cancellation in hearing aids," in *Proc. IEEE Int. Conf. Acoustics, Speech, and Signal Processing (ICASSP)*, Philadelphia, PA, USA, Mar. 2005, vol. 3, pp. 129–132.

[44] U. Forssell and L. Ljung, "Closed-loop identification revisited," *Automatica*, vol. 35, pp. 1215–1241, 1999.

[45] J. Hellgren and U. Forssell, "Bias of feedback cancellation algorithms in hearing aids based on direct closed loop identification," *IEEE Trans. Speech, Audio Processing*, vol. 9, no. 7, pp. 906–913, Nov. 2001.

[46] R. Leber and W. Schaub, "Circuit and method for the adaptive suppression of an acoustic feedback," U.S. patent, US 6611600, 2003.

[47] N. A. Shusina and B. Rafaely, "Feedback cancellation in hearing aids based on indirect closed-loop identification," in *Proc. IEEE Benelux Signal Processing Symposium (SPS)*, Leuven, Belgium, Mar. 2002, pp. 177–180.

[48] G. Rombouts, T. van Waterschoot, K. Struyve, and M. Moonen, "Acoustic feedback suppression for long acoustic paths using a nonstationary source model," *IEEE Transactions on Signal Processing*, vol. 54, no. 9, pp. 3426-3434, Sept. 2006.

[49] J. R. Deller, J. G. Proakis, and J. H. L. Hansen, *Discrete-Time Processing of Speech Signals*, Macmillan Publishing Company, Englewood Cliffs, New Jersey, 1993.

[50] N. Bisgaard and O. Dyrlund, "Acoustic feedback part 2: A digital system for suppression of feedback," *Hear. Instrum.*, vol. 42, pp. 44–45, 1991.

[51] H. R. Skovgaard, "Hearing aid compensating for acoustic feedback," US Patent, US 5680467, 1997.

[52] J. H. Stott and N. D. Wells, "Method and apparatus for reduction of unwanted feedback," US Patent, US 6269165, 2001.

Table 1: PBFD implementation of CAF.

For each block of L input samples $u[\bar{k}L+1], \ldots, u[(\bar{k}+1)L]$:

$\forall p = 0, \ldots, \frac{L_{\hat{F}}}{P} - 1:$

$$\mathbf{U}_p[\bar{k}] = \text{diag}\left\{ \boldsymbol{\mathcal{F}} \begin{bmatrix} u[(\bar{k}+1)L - pP - M + 1] \\ \vdots \\ u[(\bar{k}+1)L - pP] \end{bmatrix} \right\}.$$

Block of output samples $\mathbf{z}_{\bar{k}} = \left[z[\bar{k}L+1] \ \ldots \ z[(\bar{k}+1)L] \right]^T$:

$$\mathbf{z}_{\bar{k}} = \begin{bmatrix} \mathbf{0} & \mathbf{I}_L \end{bmatrix} \boldsymbol{\mathcal{F}}^{-1} \sum_{p=0}^{\frac{L_{\hat{F}}}{P}-1} \mathbf{U}_p[\bar{k}] \hat{\mathbf{F}}_p[\bar{k}].$$

Update formula:

$$\mathbf{y}_{\bar{k}} = \begin{bmatrix} y[\bar{k}L+1] & \ldots & y[(\bar{k}+1)L] \end{bmatrix}^T,$$

$$\mathbf{E}[\bar{k}] = \boldsymbol{\mathcal{F}} \begin{bmatrix} \mathbf{0} \\ \mathbf{I}_L \end{bmatrix} \left(\mathbf{y}_{\bar{k}} - \begin{bmatrix} \mathbf{0} & \mathbf{I}_L \end{bmatrix} \boldsymbol{\mathcal{F}}^{-1} \sum_{p=0}^{\frac{L_{\hat{F}}}{P}-1} \mathbf{U}_p[\bar{k}] \hat{\mathbf{F}}_p[\bar{k}] \right),$$

$$\hat{\mathbf{F}}_p[\bar{k}+1] = \hat{\mathbf{F}}_p[\bar{k}] + \boldsymbol{\Delta}[\bar{k}] \boldsymbol{\mathcal{F}} \mathbf{g} \boldsymbol{\mathcal{F}}^{-1} \mathbf{U}_p^H[\bar{k}] \mathbf{E}[\bar{k}].$$

Step size:

$$\boldsymbol{\Delta}[\bar{k}] = \mathit{diag}\{\mu_0[\bar{k}], \ldots, \mu_{M-1}[\bar{k}]\},$$

$$\mu_m[\bar{k}] = \frac{\bar{\mu}_m}{\sum_{p=0}^{\frac{L_{\hat{F}}}{P}-1} \left| U_{p,m}[\bar{k}] \right|^2 + \frac{L_{\hat{F}}}{P} \left| E_{p,m}[\bar{k}] \right|^2 + c}.$$

Table 2: PBFD implementation of PEMAFC-a.

For each block of L input samples $u[\bar{k}L+1], \ldots, u[(\bar{k}+1)L]$:

Block of output samples $\mathbf{z}_{\bar{k}} = \left[z[\bar{k}L+1] \ \ldots \ z[(\bar{k}+1)L]\right]^T$:

$$\mathbf{z}_{\bar{k}} = \left[\begin{array}{cc} \mathbf{0} & \mathbf{I}_L \end{array}\right] \boldsymbol{\mathcal{F}}^{-1} \sum_{p=0}^{\frac{L_{\hat{F}}}{P}-1} \mathbf{U}_p[\bar{k}]\hat{\mathbf{F}}_p[\bar{k}],$$

with

$$\mathbf{U}_p[\bar{k}] = \text{diag}\left\{\boldsymbol{\mathcal{F}}\left[\begin{array}{c} u[(\bar{k}+1)L-pP-M+1] \\ \vdots \\ u[(\bar{k}+1)L-pP] \end{array}\right]\right\}, p = 0, \ldots, \frac{L_{\hat{F}}}{P}-1.$$

Pre-filter loudspeaker and microphone signal with $A(q, \bar{k}_a - 1)$, $\bar{k}_a = \left\lceil \frac{\bar{k}L+i}{N} \right\rceil$ *(N is the framelength):*

$$\begin{aligned} u^f[\bar{k}L+i] &= A(q,\bar{k}_a-1)u[\bar{k}L+i-N], \\ y^f[\bar{k}L+i] &= A(q,\bar{k}_a-1)y[\bar{k}L+i-N],\ i=1,\ldots,L, \end{aligned}$$

$$\mathbf{U}_p^f[\bar{k}] = \text{diag}\left\{\boldsymbol{\mathcal{F}}\left[\begin{array}{c} u^f[(\bar{k}+1)L-pP-M+1] \\ \vdots \\ u^f[(\bar{k}+1)L-pP] \end{array}\right]\right\}.$$

Update AR-model $A(q, \bar{k}_a)$*:*

If $\bar{k}L+i = \bar{k}_a N$ with $\bar{k}_a$ an integer:

$$A(q,\bar{k}_a) = \text{Levinson Durbin}(\left[\begin{array}{ccc} e[\bar{k}L+i-N+1] & \ldots & e[\bar{k}L+i] \end{array}\right]^T)$$

with $e[\bar{k}L+i] = y[\bar{k}L+i] - z[\bar{k}L+i]$.

Update formula:

$$\mathbf{y}_{\bar{k}}^f = \left[\begin{array}{ccc} y^f[\bar{k}L+1] & \ldots & y^f[(\bar{k}+1)L] \end{array}\right]^T,$$

$$\mathbf{E}^f[\bar{k}] = \boldsymbol{\mathcal{F}}\left[\begin{array}{c} \mathbf{0} \\ \mathbf{I}_L \end{array}\right]\left(\mathbf{y}_{\bar{k}}^f - \left[\begin{array}{cc} \mathbf{0} & \mathbf{I}_L \end{array}\right]\boldsymbol{\mathcal{F}}^{-1}\sum_{p=0}^{\frac{L_{\hat{F}}}{P}-1}\mathbf{U}_p^f[\bar{k}]\hat{\mathbf{F}}_p[\bar{k}]\right),$$

$$\hat{\mathbf{F}}_p[\bar{k}+1] = \hat{\mathbf{F}}_p[\bar{k}] + \boldsymbol{\Delta}[\bar{k}]\boldsymbol{\mathcal{F}}\mathbf{g}\boldsymbol{\mathcal{F}}^{-1}\mathbf{U}_p^{f,H}[\bar{k}]\mathbf{E}^f[\bar{k}].$$

Step size:

$$\boldsymbol{\Delta}[\bar{k}] = \mathit{diag}\{\mu_0[\bar{k}], \ldots, \mu_{M-1}[\bar{k}]\},$$

$$\mu_m[\bar{k}] = \frac{\bar{\mu}_m}{\sum_{p=0}^{\frac{L_{\hat{F}}}{P}-1}\left|U_{p,m}^f[\bar{k}]\right|^2 + \frac{L_{\hat{F}}}{P}\left|E_{p,m}^f[\bar{k}]\right|^2 + c}.$$

Table 3: Maximum stable gain (MSG) in dB achieved with the different algorithms for a real speech signal $x[k]$. For comparison, the MSG achieved without feedback canceller is also shown (No FC).

	No FC	CAF	C-CAF	BL-CAF	PEMAFC-f	PEMAFC-a
No obstruction						
$d_G = 2$ ms	17 dB	14 dB	32 dB	31 dB	30 dB	41 dB
$d_G = 4$ ms	17 dB	33 dB	33 dB	27 dB	35 dB	37 dB
$d_G = 6$ ms	16 dB	27 dB	31 dB	35 dB	37 dB	39 dB
Mobile phone						
$d_G = 2$ ms	9 dB	16 dB	17 dB	27 dB	33 dB	39 dB
$d_G = 4$ ms	9 dB	31 dB	22 dB	26 dB	38 dB	38 dB
$d_G = 6$ ms	10 dB	27 dB	23 dB	27 dB	37 dB	39 dB

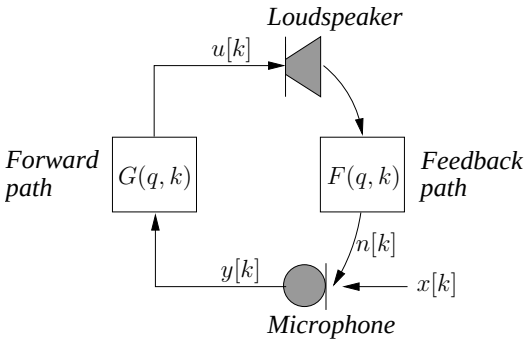

Figure 1: Acoustic feedback.

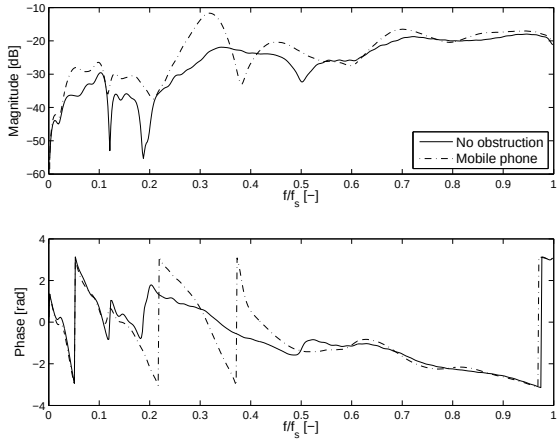

Figure 2: Feedback path frequency response of a commercial, GN ReSound behind-the-ear hearing aid connected to a vented earmold (with a vent size of 2 mm) for two conditions, i.e., without obstruction and with a mobile phone attached to the ear.

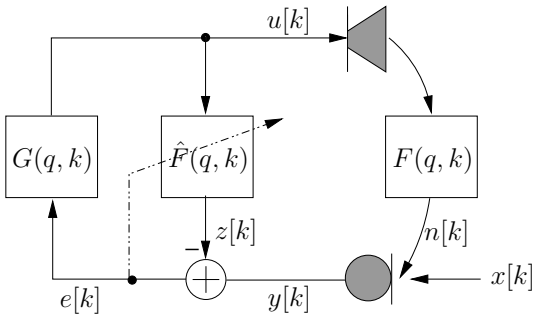

Figure 3: Adaptive feedback cancellation.

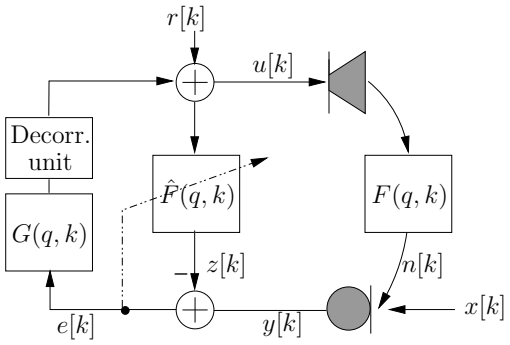

Figure 4: CAF with decorrelating signal operations (i.e., inserting a decorrelation unit or adding a probe signal $r[k]$).

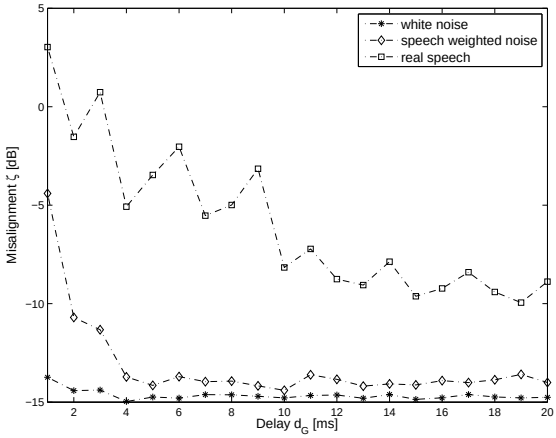

Figure 5: Misalignment of the PBFD CAF as a function of the delay d_G for white noise, speech weighted noise and real speech as a desired signal. $G(q,k) = Gq^{-d_G}$ with $G = 10$ dB.

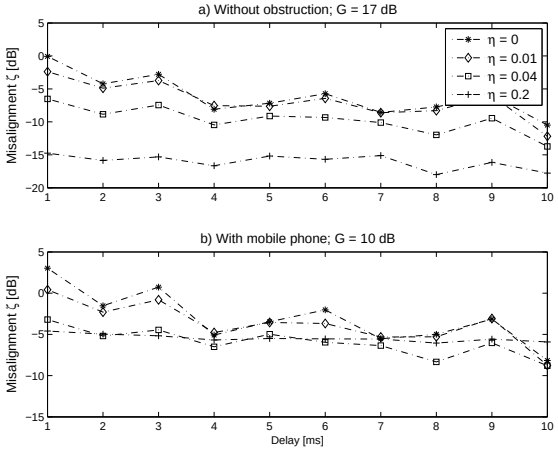

Figure 6: Misalignment of the C-CAF as a function of the delay d_G of $G(q,k) = Gq^{-d_G}$ for different settings of η and real speech as a desired signal. a) Without obstruction ($G = 17$ dB); b) With a mobile phone attached to the head ($G = 10$ dB).

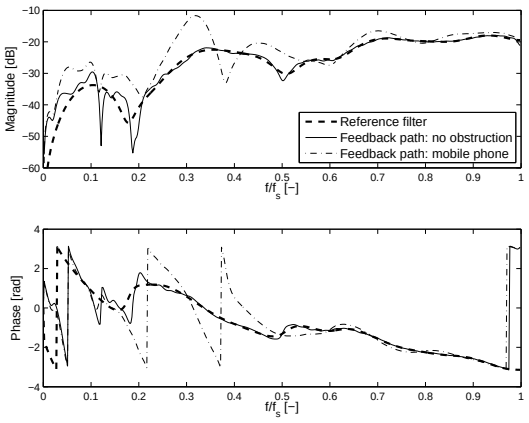

Figure 7: Frequency response of the reference filter $\hat{\mathbf{f}}_{ref}$ used in the C-CAF. For comparison, the true feedback path for the scenario without obstruction and with a mobile phone are also depicted.

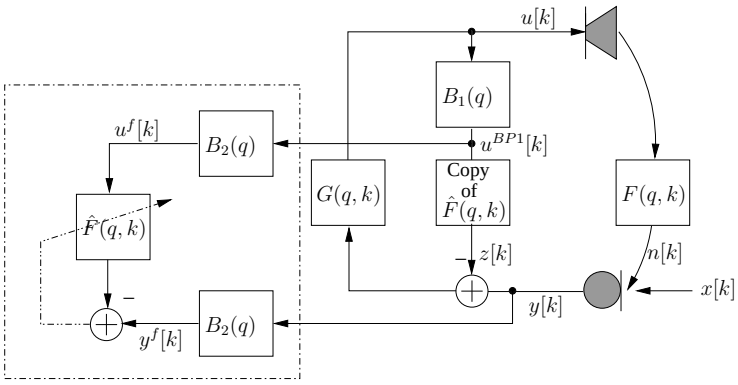

Figure 8: Bandlimited adaptive feedback cancellation (BL-CAF).

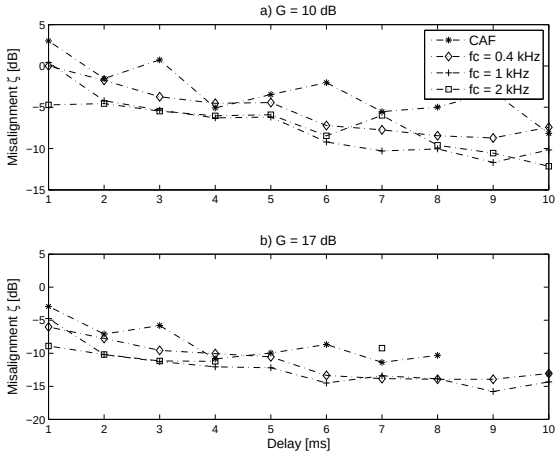

Figure 9: Misalignment of BL-CAF as a function of the delay d_G for different cut-off frequencies f_c (i.e., $f_c = 0.4$ kHz, $f_c = 1$ kHz and $f_c = 2$ kHz) and real speech as a desired signal. a) $G = 10$ dB; b) $G = 17$ dB (for $d_G = 5 - 6$ ms and $d_G = 8 - 10$ ms, instability occurs for the BL-CAF with $f_c = 2$ kHz; for $d_G = 9 - 10$ ms, instability occurs for the CAF).

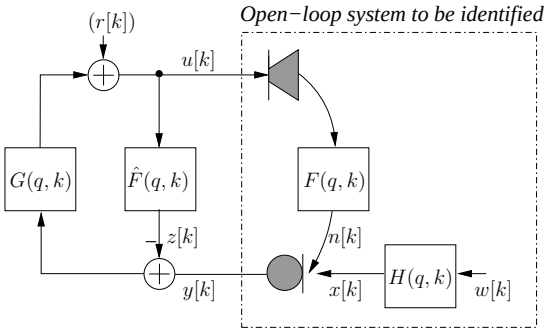

Figure 10: Closed-loop system set-up.

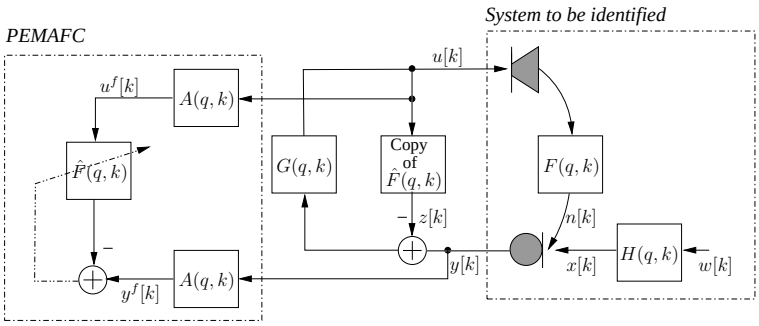

Figure 11: Feedback cancellation with the prediction error method (PEMAFC).

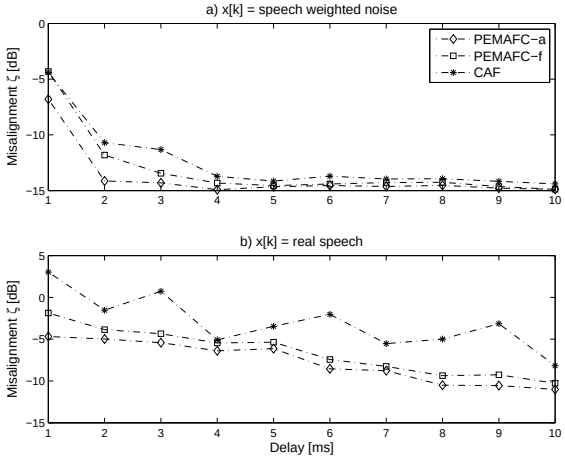

Figure 12: Misalignment of the PEMAFC with a fixed (PEMAFC-f) and adaptive AR model (PEMAFC-a) as a function of the delay d_G for the acoustic feedback path with a mobile phone attached to the head. a) $x[k]$ = speech weighted noise; b) $x[k]$= real speech.

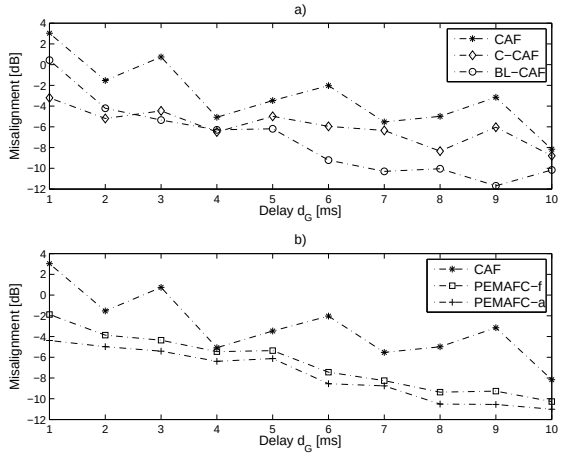

Figure 13: Comparison of steady-state performance as a function of the delay d_G of $G(q,k)$ ($G = 10$ dB) for the acoustic feedback path with mobile phone attached to the head. a) Misalignment of the CAF, the C-CAF and the BL-CAF; b) Misalignment of the CAF, the PEMAFC-f and the PEMAFC-a; Real speech as a desired signal $x[k]$.

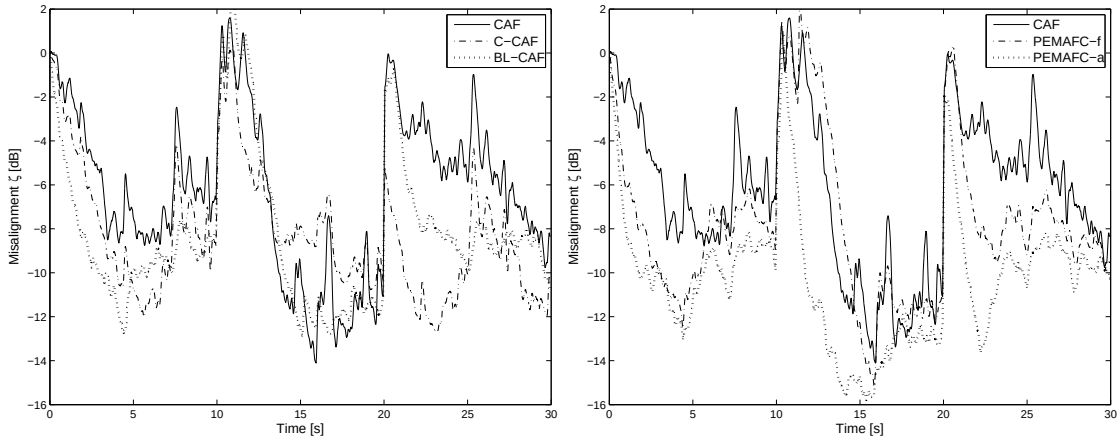

(a) (b)

Figure 14: Convergence and tracking performance of the different algorithms. At 10 s and 20 s a sudden change in the feedback path occurs. a) Misalignment as a function of time of the CAF, the C-CAF and the BL-CAF; b) Misalignment as a function of time of the CAF, the PEMAFC-f and the PEMAFC-a.